

---

# (De)Randomized Smoothing for Certifiable Defense against Patch Attacks

---

Alexander Levine<sup>1</sup> Soheil Feizi<sup>1</sup>

## Abstract

Patch adversarial attacks on images, in which the attacker can distort pixels within a region of bounded size, are an important threat model since they provide a quantitative model for physical adversarial attacks. In this paper, we introduce a certifiable defense against patch attacks that guarantees for a given image and patch attack size, no patch adversarial examples exist. Our method is related to the broad class of *randomized smoothing* robustness schemes which provide high-confidence probabilistic robustness certificates. By exploiting the fact that patch attacks are more constrained than general sparse attacks, we derive meaningfully large robustness certificates. Additionally, the algorithm we propose is derandomized, providing deterministic certificates. To the best of our knowledge, there exists only one prior method for certifiable defense against patch attacks, which relies on interval bound propagation. While this sole existing method performs well on MNIST, it has several limitations: it requires computationally expensive training, does not scale to ImageNet, and performs poorly on CIFAR-10. In contrast, our proposed method effectively addresses all of these issues: our classifier can be trained quickly, achieves high clean and certified robust accuracy on CIFAR-10, and provides certificates at the ImageNet scale. For example, for a  $5 \times 5$  patch attack on CIFAR-10, our method achieves up to around 57.8% certified accuracy (with a classifier around 83.9% clean accuracy), compared to at most 30.3% certified accuracy for the existing method (with a classifier with around 47.8% clean accuracy), effectively establishing a new state-of-the-art. Code is available at <https://github.com/alevine0/patchSmoothing>.

## 1. Introduction

In recent years, adversarial attacks have become a topic of great interest in machine learning. (Szegedy et al., 2013; Madry et al., 2017; Carlini & Wagner, 2017) However, in many instances the threat models considered for these attacks, such as small  $L_\infty$  distortions to every pixel of an image, implicitly require the attacker to be able to directly interfere with the input to a neural network: this represents only a limited practical threat. (We recognize that (Kurakin et al., 2018) has shown that  $L_\infty$  attacks may be effective even when the distorted image has been printed and re-photographed, but this is clearly a limited setting.) However, the development of *physical* adversarial attacks (Eykholt et al., 2018), in which small visible changes are made to real world objects in order to disrupt classification of images of these objects, represents a more concerning security threat.

Physical adversarial attacks can often be modeled as *patch* adversarial attacks, in which the attacker can make arbitrary changes to pixels within a region of bounded size. Indeed, there is often a direct relationship between the two: for example, the universal patch attack proposed by (Brown et al., 2017) is effective as a physical sticker. In that attack, the pixels of the attack do not depend on the attacked image. Image-specific patch attacks have also been proposed, such as LaVAN (Karmon et al., 2018), which reduces ImageNet classification accuracy to 0% using only a  $42 \times 42$  pixel square patch (on images of size  $299 \times 299$ ). In this paper, we also consider attacks on square patches, of size  $m \times m$ .

Practical defenses against patch adversarial attacks have been proposed (Hayes, 2018; Naseer et al., 2018). For the aforementioned  $42 \times 42$  pixel attacks on ImageNet, (Naseer et al., 2018) claims the current state-of-the-art practical defense. However, (Chiang et al., 2020) has recently broken this defense, reducing classification accuracy on ImageNet to 14%. In the same work, (Chiang et al., 2020) also proposes the first *certified* defense against patch adversarial attacks, which uses interval bound propagation (Gowal et al., 2018). In a certifiably robust classification scheme, in addition to providing a classification for each image, the classifier may also return an assurance that the classification will provably not change under any distortion of a certain magnitude and threat model. One then both reports the *clean accuracy* (normal accuracy) of the model,

---

<sup>1</sup>Department of Computer Science, University of Maryland, College Park, MD. Correspondence to: Alexander Levine <alevine0@cs.umd.edu>, Soheil Feizi <sfeizi@cs.umd.edu>.

as well as the *certified accuracy* (percent of images which are both correctly classified, and for which it is guaranteed that the classification will not change under a certain attack type). Certified defenses are preferable to practical defenses because they guarantee that *no* future adversary (under a certain threat model) will be effective against the defense.

The certified defense proposed by (Chiang et al., 2020), however, can not defend against the attack proposed by (Chiang et al., 2020). Specifically, while this certified defense performs well on MNIST, it achieves poor certified accuracy on CIFAR-10 and, to quote, “is unlikely to scale to ImageNet.” In this work, we propose a certified defense against patch adversarial attacks which overcomes these issues:

Dataset and Attack Size	Chiang et al. Certified Acc (Clean Acc)	Our method Certified Acc (Clean Acc)
MNIST $5 \times 5$	<b>60.4%</b> (92.0%)	52.83% (96.66%)
CIFAR $5 \times 5$	30.3% (47.8%)	<b>57.83%</b> (83.93%)
ImageNet $42 \times 42$	N/A	<b>14.5%</b> (43.1%)

Table 1. Comparison of the certified accuracy of our defense scheme, versus (Chiang et al., 2020). For each technique, we report the certified and clean accuracies of the model with parameters giving the highest certified accuracy.

We note that our method has top-1 *certified* accuracy on ImageNet classification which is approximately equal to the 14% *empirical* accuracy of the state-of-the-art practical defense (Naseer et al., 2018) under the attack proposed by (Chiang et al., 2020) (although our clean accuracy is lower, 43% vs. 71%). The certified defense proposed by (Chiang et al., 2020) also has a computationally expensive training algorithm: the training time for the reported best model was 8.4 GPU hours using NVIDIA 2080 Ti GPUs. Our MNIST models, by contrast, took approximately 1.0 GPU hour to train on the same model of GPU.

Our certifiably robust classification scheme is based on *randomized smoothing*, a class of techniques for certifiably robust classification which has been proposed for various threat models, including  $L_2$  (Li et al., 2018; Cohen et al., 2019; Salman et al., 2019),  $L_1$  (Lecuyer et al., 2019; Teng et al., 2020),  $L_0$  (Lee et al., 2019; Levine & Feizi, 2019a), and Wasserstein (Levine & Feizi, 2019b) metrics. All of these methods rely on a similar mechanism where noisy versions of an input image  $\mathbf{x}$  are used in the classification. Such noisy inputs are created either by adding random noise to all pixels (Lecuyer et al., 2019) or by removing (*ablating*) some of the pixels (Levine & Feizi, 2019a). A large number of noisy images are then classified by a *base classifier* and then the consensus of these classifications is reported as the

final classification result. For an adversarial image  $\mathbf{x}'$  at a bounded distance from  $\mathbf{x}$ , the probability distributions of possible noisy images which can be produced from  $\mathbf{x}$  and  $\mathbf{x}'$  will substantially overlap. This implies that, if a sufficiently large fraction of noisy images derived from  $\mathbf{x}$  are classified to some class  $c$ , then with high probability, a plurality of noisy images derived from  $\mathbf{x}'$  will also be assigned to this class. While recent work (Kumar et al., 2020; Blum et al., 2020; Yang et al., 2020) has shown that these techniques may not extend to certain metrics (particularly the  $L_\infty$  metric) in the classification setting, randomized smoothing has also been extended to protect against threat models beyond inference-time attacks on classification, to defend against attacks on machine learning interpretation (Levine et al., 2019) and poisoning attacks (Rosenfeld et al., 2020).

In this paper, we focus on *patch adversarial attacks* which can be considered as a special case of  $L_0$  (sparse) adversarial attacks: in an  $L_0$  attack, the adversary can choose a limited number of pixels and apply unbounded distortions to them. A patch adversarial attack is therefore a restricted version of a sparse adversarial attack: the attacker is additionally constrained to selecting only a block of adjacent pixels to attack, rather than any arbitrary pixels.

The current state-of-the-art certified defense against sparse adversarial attacks is a randomized smoothing method proposed by (Levine & Feizi, 2019a). In this method, a base classifier,  $f(\mathbf{x})$ , is trained to make classifications based on only a small number of randomly-selected pixels: the rest of the image is *ablated*, meaning that it is encoded as a null value. At test time, the final classification  $g(\mathbf{x})$  is taken as the class most likely to be returned by  $f$  on a randomly ablated version of the image. (In practice,  $g$  is estimated by evaluating  $f$  on large random samples of possible ablations.) Note that *regardless of the choice of pixels that an adversary might distort*, the probability that any of these pixels is also one of the pixels present in each particular ablated sample used by the base classifier is bounded. Then if the base classifier returns the correct classification on a sufficiently large proportion of ablated images, one can conclude that no adversarial examples with fewer than a certain number of distorted pixels exist.

In practice, we find that applying this scheme directly to patch attacks yields poor results (Table 2). This is because the defense proposed in (Levine & Feizi, 2019a) does not incorporate the additional structure of the attack. In particular, for patch attacks, we can use the fact that the attacked pixels form a contiguous square to develop a more effective defense. In this paper, we propose a *structured ablation* scheme, where instead of independently selecting pixels to use for classification, we select pixels in a correlated way in order to reduce the probability that the adversarial patch is sampled. In Theorems 1 and 2, we characterize the robust-

ness certificates of proposed structured ablation methods against patch adversarial attacks. Empirically, structured ablation certificates yields much improved certified accuracy to patch attacks, compared to the naive  $L_0$  certificate. (52.83% for  $5 \times 5$  patches on MNIST, compared to 8.04%.)

By reducing the total number of possible ablations of an image, structured ablation also allows us to de-randomize our algorithm, yielding improved, deterministic certificates. For  $L_0$  robustness, (Levine & Feizi, 2019a) achieves the largest median certificates on MNIST by using a base classifier  $f$  which classifies using only 45 out of 784 pixels. Note that there are  $\binom{784}{45} \approx 4 \times 10^{73}$  ways to make this selection. It is therefore not feasible to evaluate precisely the probability that  $f(\mathbf{x})$  returns any particular class  $c$ : one must estimate this based on random samples, following techniques originally developed by (Cohen et al., 2019) for  $L_2$  randomized smoothing. Using our proposed methods, the number of possible ablations is small enough so that it is tractable to classify using all possible ablations: we can *exactly* evaluate the probability that  $f(\mathbf{x})$  returns each class. Our certificate is therefore exact, rather than probabilistic: we know what  $f$  returns given each possible ablated image as input, and we know the maximum number of these classifications which could possibly be distorted by the adversary, so we can determine whether or not the plurality classification could change using simple counting. Determinism provides additional benefits, which we explore in Sections 2.6 and 3.2. In a concurrent work, (Rosenfeld et al., 2020) has also independently proposed a de-randomized version of a randomized smoothing technique. However, the threat model of that work is quite different: (Rosenfeld et al., 2020) develops a smoothing defense against label-flipping poisoning (training-time) attacks, where the adversary is able to change the label of a bounded number of training samples. Notably, (Rosenfeld et al., 2020)’s result only applies directly to linear base classifiers (although in the particular threat model considered, the inputs to this linear classifier may be nonlinear features learned from the unlabeled training data, which the adversary cannot perturb). By restricting to linear classifiers, (Rosenfeld et al., 2020) is able to analytically determine the probabilities of  $f(\mathbf{x})$  returning each class. By contrast, our de-randomized smoothing technique for inference-time patch attacks makes no restriction on the architecture of the base classifier  $f$ , in practice a deep convolutional network.

## 2. Certifiable Defenses against Patch Attacks

### 2.1. Sparse Ablation (Levine & Feizi, 2019a)

As mentioned in the introduction, patch attacks can be regarded as a restricted case of  $L_0$  attacks. In particular, let  $\rho$  be the magnitude of an  $L_0$  adversarial attack: the attacker modifies  $\rho$  pixels and leaves the rest unchanged. A patch

attack, with an  $m \times m$  adversarial patch, is also an  $L_0$  attack, with  $\rho = m^2$ . We can then attempt to apply existing certifiably robust classification schemes for the  $L_0$  threat model to the patch attack threat model: we simply need to certify to an  $L_0$  radius of  $\rho = m^2$ . Consider specifically the  $L_0$  smoothing-based certifiably robust classifier introduced by (Levine & Feizi, 2019a). In this classification scheme, given an input image  $\mathbf{x}$ , the base classifier  $f$  classifies a large number of distinct randomly-ablated versions of  $x$ , in each of which only  $k$  pixels of the original image are randomly and independently selected to be retained and used by the base classifier  $f$ . Therefore, for *any choice* of  $\rho$  pixels that the attacker could choose to attack, the probability that any of these  $\rho$  pixels is also one of the  $k$  pixels used in  $f$ ’s classification is:

$$\begin{aligned} \Delta &:= \Pr(f \text{ uses attacked pixels}) \\ \Delta &= 1 - \frac{\binom{hw-\rho}{k}}{\binom{hw}{k}} \approx k \frac{\rho}{hw} = \frac{km^2}{hw} \quad (k, \rho \ll hw) \end{aligned}$$

where  $\rho$  is the number of attacked pixels,  $k$  is the number of retained pixels used by the base classifier, and the overall dimensions of the input image  $\mathbf{x}$  are  $h \times w$ . To understand this, note that the classifier has  $k$  opportunities to choose an attacked pixel, and  $\rho$  out of  $hw$  pixels are attacked. Clearly, if  $f$  does not use any of the attacked pixels, then its output will not be corrupted by the attacker. Therefore, the attacker can change the output of  $f(\mathbf{x})$  with probability at most  $\Delta$ . Let  $c$  be the majority classification at  $\mathbf{x}$  (i.e.,  $g(\mathbf{x}) = c$ ). If  $f(\mathbf{x}) = c$  with probability greater than  $0.5 + \Delta$ , then for any distorted image  $\mathbf{x}'$ , one can conclude that  $f(\mathbf{x}') = c$  with probability greater than 0.5, and therefore that  $g(\mathbf{x}') = c$ . While this technique produces state-of-the-art guarantees against general  $L_0$  attacks, it yields rather poor certified accuracies when applied to patch attacks, because it does not take advantage of the structure of the attack (Table 2).

Retained pixels $k$	Classification accuracy	Certified accuracy
5	32.32%	8.04%
10	74.90%	5.73%
15	86.09%	4.53%
20	90.29%	0.15%
25	93.05%	0

Table 2. Certified accuracy to  $5 \times 5$  adversarial patches on MNIST from directly applying  $L_0$  smoothing as proposed by (Levine & Feizi, 2019a). Note that with  $L_0$  smoothing, the geometry of the attack is not taken into consideration: these are therefore actually certified accuracies for any  $L_0$  attack on up to  $\rho = 25$  pixels. The certificates are probabilistic, with 95% confidence.

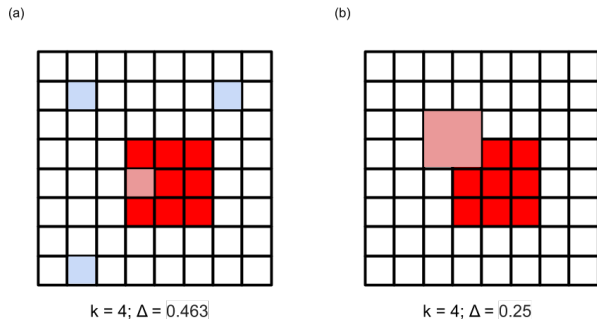


Figure 1. Likelihood of selecting a pixel which is part of the attacked patch (red) for (a) sparse randomized ablation, as proposed by (Levine & Feizi, 2019a) (b) Structured ablation, using a block of size  $s = 2$ . In both cases,  $k = 4$  pixels are retained. However, in the sparse case, if *any* of the four independently-selected pixels sample the patch, then the classification may be impacted: this occurs with probability  $\Delta = 1 - \binom{64-9}{4} / \binom{64}{4} \approx 0.463$ . In contrast, the probability that the block overlaps with the adversarial patch is only  $\frac{16}{64} = 0.25$ .

## 2.2. Structured Ablation

In order to exploit the restricted nature of patch attacks, we propose two *structured ablation* methods, which select correlated groups of pixels in order to reduce the probability  $\Delta$  that the adversarial patch is sampled:

- **Block Smoothing:** In this method, we select a single  $s \times s$  square block of pixels, and ablate the rest of the image. The number of retained pixels is then  $k = s^2$ . Note that for an  $m \times m$  adversarial patch, out of the  $h \times w$  possible selections for blocks to use for classification,  $(m + s - 1)^2$  of them will intersect the patch. Then we have:

$$\Delta_{\text{block}} = \frac{(m + s - 1)^2}{hw} = \frac{(m + \sqrt{k} - 1)^2}{hw} < \frac{4 \max(m^2, k)}{hw}. \quad (1)$$

As illustrated in Figure 1, this implies a substantially decreased probability of intersecting the adversarial patch, compared to sampling  $k$  pixels independently.

- **Band Smoothing:** In this method, we select a single band (a column or a row) of pixels of width  $s$ , and ablate the rest of the image. In the case of a column, the number of retained pixels is then  $k = sh$ . For an  $m \times m$  adversarial patch, out of the  $w$  possible selections for bands to use for classification,  $m + s - 1$  of them will intersect the patch. Then we have:

$$\Delta_{\text{col.}} = \frac{m + s - 1}{w} = \frac{m + k/h - 1}{w} < \frac{\max(hm, k)}{hw}. \quad (2)$$

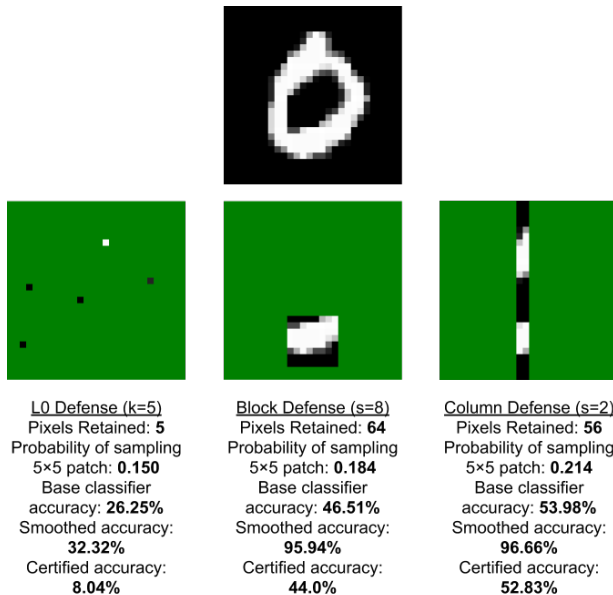


Figure 2. Comparison of the  $L_0$  defense proposed by (Levine & Feizi, 2019a) to our proposed defenses on MNIST, for a  $5 \times 5$  patch attack. While sampling a single block or band slightly increases the probability  $\Delta$  that an adversarially distorted pixel is used, the large increase in the total number of retained pixels, and therefore the base classifier accuracy, more than makes up for this increase in  $\Delta$ . However, the number of retained pixels alone does not perfectly correspond to higher base classifier accuracy: while the band method uses slightly fewer pixels than the block method, the base classifier has substantially higher accuracy, leading to higher certified accuracy. For each method, we use hyperparameters optimized for highest certified robust accuracy. Note that the  $L_0$  certificate is probabilistic (with 95% confidence) while our certificates are deterministic.

For both of these methods, it is tractable to use the base classifier to classify all possible ablated versions of an image (there are  $hw$  possible ablations for block smoothing, and  $w$  for column smoothing): this allows us to exactly compute  $g(\mathbf{x})$ , and to compute deterministic certificates. Our experiments show that structured ablation produces higher certified accuracy than  $L_0$  sparse ablation. This is because, for similar values of  $\Delta$ , structured ablation methods yield much higher base classifier accuracies. (Figure 2). Empirically, we find that the band method (and specifically, column smoothing) produces the most certifiably robust classifiers (Tables 4,5). In Section 3.3, we explore structured ablation using multiple blocks or bands of pixels.

## 2.3. Notation for Algorithms

Following the notation of (Levine & Feizi, 2019a), let  $\mathcal{S}$  be the set of possible values for a pixel in an input image. Because our base classifier only uses a subset of the image, we must have a way to encode missing pixels: let NULL represent the absence of information about a pixel, and let  $\mathcal{S}_{\text{NULL}}$

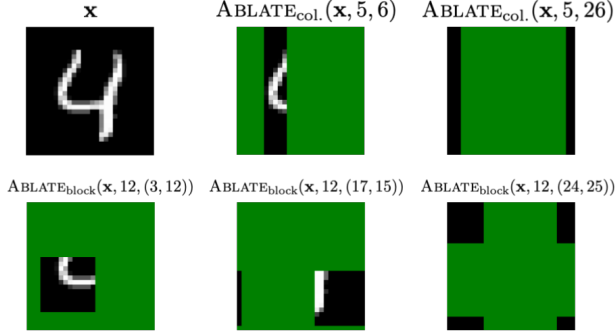


Figure 3. Function of the ABLATE operators. Ablated pixels are represented in green. Note that the retained regions wrap around.

be the set  $\mathcal{S} \cup \{\text{NULL}\}$ . Let  $n$  be the number of classes in the classification problem. We will assume that our base classifier  $f$  is a deterministic function in  $\mathcal{S}_{\text{NULL}}^{h \times w} \rightarrow [0, 1]^n$ , with  $\sum_{i=0}^{n-1} f_i(\cdot) = 1$ . In other words, the base classifier will take an image with some pixels ablated to NULL and others retained, and output *softmaxed* logits representing the confidence that the classifier has in each class. As a practical matter,  $f$  can easily be represented as a neural network: we encode the additional NULL symbol in the input in the same manner described by (Levine & Feizi, 2019a) for each dataset tested. For the block smoothing method, we will define the operation  $\text{ABLATE}_{\text{block}}(\mathbf{x}, s, (i, j))$ , which will take an image  $\mathbf{x} \in \mathcal{S}^{h \times w}$ , and return an ablated image in  $\mathcal{S}_{\text{NULL}}^{h \times w}$  that retains only the pixels in a  $s \times s$  block with upper-left corner  $(i, j)$ , and ablates the rest. For the column (or row, by symmetry) smoothing method, similarly define  $\text{ABLATE}_{\text{col}}(\mathbf{x}, s, i)$ , which retains only a column of width  $s$  starting at  $x = i$ . In both cases, if the retained block or column would extend beyond the size of the image, the retained region will wrap around; see Figure 3. (This is necessary to ensure that an adversarial patch at the center of an image is not more likely to be sampled than one at the edge of the image.)

Additionally we define  $\text{STABLEARGSORT}$  of a list to return the indices that would sort the list in descending order, such that, in the event of a tie, the lower index is listed first. For example  $\text{STABLEARGSORT}([3, 23, 23, 7]) = [1, 2, 3, 0]$ .

#### 2.4. Block Smoothing Algorithm

The “block” variation of our algorithm is presented as Algorithm 1. In short, we evaluate the base classifier on all possible blocks. On each input, rather than simply taking the maximum class returned by the base classifier, we count every class for which the logit exceeds a threshold  $\theta$ . The classifier can abstain entirely if no class reaches this threshold (for example if the block contains no useful information). If the gap in the counts between the top class and the next

---

#### Algorithm 1 Block Smoothing

---

**Inputs:** Base classifier  $f \in \mathcal{S}_{\text{NULL}}^{h \times w} \rightarrow [0, 1]^n$ , image  $\mathbf{x}$ , block size  $s$ , attack size  $m$ , threshold  $\theta$ .  
**Outputs:** class  $c$ , boolean *certified?*  
Counts  $\leftarrow [0 \dots 0]$  ( $n$  zeroes)  
**for all**  $(i, j)$  in  $0 \leq i < w, 0 \leq j < h$  **do**  
  Logits  $\leftarrow f(\text{ABLATE}_{\text{block}}(\mathbf{x}, s, (i, j)))$   
  **for all**  $k$  in  $0 \leq k < n$  **do**  
    **if** Logits[ $k$ ]  $> \theta$  **then**  
      Counts[ $k$ ]  $+$  = 1  
    **end if**  
  **end for**  
**end for**  
AffectedBlocks  $\leftarrow (m + s - 1)^2$   
SortedClasses  $\leftarrow \text{STABLEARGSORT}(\text{Counts})$   
 $c \leftarrow \text{SortedClasses}[0]$   
 $c_{\text{next}} \leftarrow \text{SortedClasses}[1]$   
**if** Counts[ $c$ ]  $>$  Counts[ $c_{\text{next}}$ ]  $+ 2 \times \text{AffectedBlocks}$  **then**  
  *certified?*  $\leftarrow \text{True}$   
**else if** Counts[ $c$ ] = Counts[ $c_{\text{next}}$ ]  $+ 2 \times \text{AffectedBlocks}$   
**and**  $c < c_{\text{next}}$  **then**  
  *certified?*  $\leftarrow \text{True}$   
**else**  
  *certified?*  $\leftarrow \text{False}$   
**end if**  
**Return**  $c, \text{certified?}$

---

class is greater than twice the number of classifications which could possibly be affected by an  $m \times m$  adversarial patch, then we can certify that no such patch can change the final smoothed classification output  $c$ . During training, as in prior smoothing works, we train  $f$  on ablated samples, using a single randomly-determined ablation pattern (selection of block to retain) on all samples in each batch.

**Theorem 1.** *For any image  $\mathbf{x}$ , base classifier  $f$ , smoothing block size  $s$ , and threshold  $\theta$ , if Algorithm 1 returns class  $c$  on input  $\mathbf{x}$  and certifies this classification, then Algorithm 1 will return class  $c$  on all inputs  $\mathbf{x}'$  that differ from  $\mathbf{x}$  only within an  $m \times m$  region of pixels.*

*Proof.* Let  $(i', j')$  represent the upper-right corner of the  $m \times m$  patch in which  $\mathbf{x}$  and  $\mathbf{x}'$  differ. Note that the output of  $\text{ABLATE}_{\text{block}}(\mathbf{x}, s, (i, j))$  will be equal to the output of  $\text{ABLATE}_{\text{block}}(\mathbf{x}', s, (i, j))$ , unless the  $s \times s$  block retained (starting at  $(i, j)$ ) intersects with the  $m \times m$  adversarial patch (starting at  $(i', j')$ ). This condition occurs only when both  $i$  is in the range between  $i' - s + 1$  and  $i' + m - 1$ , inclusive, and  $j$  is in the range between  $j' - s + 1$  and  $j' + m - 1$ , inclusive. Note that there are  $(s + m - 1)$  values each for  $i$  and  $j$  which meet this condition, and therefore  $(s + m - 1)^2$  such pairs  $(i, j)$ . Therefore  $\text{ABLATE}_{\text{block}}(\mathbf{x}', s, (i, j)) = \text{ABLATE}_{\text{block}}(\mathbf{x}, s, (i, j))$  in all but  $(s + m - 1)^2$  cases.

(If  $i' - s + 1 < 0$ , then the intersecting values for  $i$ , taking into account the wrapping behavior of the ABLATE operator, will be  $h - (i' - s + 1)$  through  $h$  and 0 through  $i' + m - 1$ : there are still  $(s + m - 1)$  such values, and similar logic applies to  $j'$ .)

As a consequence,  $f(\text{ABLATE}_{\text{block}}(\mathbf{x}, s, (i, j)))$  will equal  $f(\text{ABLATE}_{\text{block}}(\mathbf{x}', s, (i, j)))$  in all but  $(s + m - 1)^2$  cases, so the Counts which are incremented will be the same in all but at most  $(s + m - 1)^2$  (= AffectedBlocks) iterations. Let  $\text{Counts}_{\mathbf{x}}$  and  $\text{Counts}_{\mathbf{x}'}$  represent the state of the Counts array after the main loop of the algorithm on inputs  $\mathbf{x}$  and  $\mathbf{x}'$ , respectively, and similarly define  $c_{\mathbf{x}}$ ,  $c_{\mathbf{x}'}$ , and  $c_{\text{next}_{\mathbf{x}}}$ . Because, for each class  $k$ ,  $\text{Counts}[k]$  is incremented by at most 1 per iteration, we have that:

$$|\text{Counts}_{\mathbf{x}}[k] - \text{Counts}_{\mathbf{x}'}[k]| \leq \text{AffectedBlocks}. \quad (3)$$

If  $\text{Counts}_{\mathbf{x}}[c_{\mathbf{x}}] > \text{Counts}_{\mathbf{x}}[c_{\text{next}_{\mathbf{x}}}] + 2 \times \text{AffectedBlocks}$ , then by sorting, we have that for all classes  $k \neq c_{\mathbf{x}}$ ,  $\text{Counts}_{\mathbf{x}}[c_{\mathbf{x}}] > \text{Counts}_{\mathbf{x}}[k] + 2 \times \text{AffectedBlocks}$ . Then by Equation 3,  $\text{Counts}_{\mathbf{x}'}[c_{\mathbf{x}}] > \text{Counts}_{\mathbf{x}'}[k]$ , and so  $c_{\mathbf{x}'} = c_{\mathbf{x}}$ .

If  $\text{Counts}_{\mathbf{x}}[c_{\mathbf{x}}] = \text{Counts}_{\mathbf{x}}[c_{\text{next}_{\mathbf{x}}}] + 2 \times \text{AffectedBlocks}$  and  $c_{\mathbf{x}} < c_{\text{next}_{\mathbf{x}}}$  then for all  $k \neq c_{\mathbf{x}}$ ,  $\text{Counts}_{\mathbf{x}}[c_{\mathbf{x}}] \geq \text{Counts}_{\mathbf{x}}[k] + 2 \times \text{AffectedBlocks}$ . In the inequality case, we already have that  $\text{Counts}_{\mathbf{x}'}[c_{\mathbf{x}}] > \text{Counts}_{\mathbf{x}'}[k]$ . For the equality case, consider any class  $k$  for which  $\text{Counts}_{\mathbf{x}}[c_{\mathbf{x}}] = \text{Counts}_{\mathbf{x}}[k] + 2 \times \text{AffectedBlocks}$ . Note that  $\text{Counts}_{\mathbf{x}}[c_{\text{next}_{\mathbf{x}}}] = \text{Counts}_{\mathbf{x}}[k]$  and also, by stable sorting of  $\text{Counts}_{\mathbf{x}}$ ,  $c_{\text{next}_{\mathbf{x}}} \leq k$ . Then because  $c_{\mathbf{x}} < c_{\text{next}_{\mathbf{x}}}$ , we have that  $c_{\mathbf{x}} < k$ . By Equation 3,  $\text{Counts}_{\mathbf{x}'}[c_{\mathbf{x}}] \geq \text{Counts}_{\mathbf{x}'}[k]$ . Then, by stable sorting of  $\text{Counts}_{\mathbf{x}'}$ ,  $c_{\mathbf{x}'} = c_{\mathbf{x}}$ .  $\square$

## 2.5. Column Smoothing Algorithm

The column version of our algorithm is presented as Algorithm 2. (An algorithm using rows rather than columns can be derived by simply transposing the input). Note that this algorithm is nearly identical to the block variation: the difference is that we only need to consider  $w$  rows rather than  $hw$  blocks. Formally, we claim that:

**Theorem 2.** *For any image  $\mathbf{x}$ , base classifier  $f$ , smoothing column size  $s$ , and threshold  $\theta$ , if Algorithm 2 returns class  $c$  on input  $\mathbf{x}$  and certifies this classification, then Algorithm 2 will return class  $c$  on all inputs  $\mathbf{x}'$  that differ from  $\mathbf{x}$  only within an  $m \times m$  region of pixels.*

This theorem can be proved similarly to Theorem 1.

## 2.6. Changes from Standard Randomized Smoothing

In conventional randomized smoothing algorithms (Lecuyer et al., 2019; Levine & Feizi, 2019a; Cohen et al., 2019; Salman et al., 2019), rather than computing the probability that  $f$  returns each class directly by exhaustive iteration,

---

### Algorithm 2 Band (Column) Smoothing

---

**Inputs:** Base classifier  $f \in \mathcal{S}_{\text{NULL}}^{h \times w} \rightarrow [0, 1]^n$ , image  $\mathbf{x}$ , column size  $s$ , attack size  $m$ , threshold  $\theta$ .

**Outputs:** class  $c$ , boolean *certified?*

Counts  $\leftarrow [0 \dots 0]$  ( $n$  zeroes)

**for all**  $i$  in  $0 \leq i < w$  **do**

Logits  $\leftarrow f(\text{ABLATE}_{\text{col}}(\mathbf{x}, s, i))$

**for all**  $k$  in  $0 \leq k < n$  **do**

**if** Logits[ $k$ ]  $> \theta$  **then**

Counts[ $k$ ]  $+$  = 1

**end if**

**end for**

**end for**

AffectedBands  $\leftarrow m + s - 1$

SortedClasses  $\leftarrow \text{STABLEARGSORT}(\text{Counts})$

$c \leftarrow \text{SortedClasses}[0]$

$c_{\text{next}} \leftarrow \text{SortedClasses}[1]$

**if** Counts[ $c$ ]  $> \text{Counts}[c_{\text{next}}] + 2 \times \text{AffectedBands}$  **then**

*certified?*  $\leftarrow \text{True}$

**else if** Counts[ $c$ ] = Counts[ $c_{\text{next}}] + 2 \times \text{AffectedBands}$

**and**  $c < c_{\text{next}}$  **then**

*certified?*  $\leftarrow \text{True}$

**else**

*certified?*  $\leftarrow \text{False}$

**end if**

**Return**  $c, \text{certified?}$

---

one must instead lower-bound, with high confidence, the probability  $p_c$  that  $f$  returns the plurality class  $c$  and upper-bound the probabilities  $p_{c'}$  that  $f$  returns all other classes, based on samples. This leads to decreased certified accuracy due to estimation error. Additionally, all of these bounds must hold simultaneously: in order to ensure with high confidence that the gap between  $p_c$  and  $p_{c'}$  is sufficiently large for each  $c'$  to prove robustness, one must bound the population probabilities for *every* class. (Lecuyer et al., 2019) does this directly using a union bound, leading to increased error as the number of classes increases. However, later works, following (Cohen et al., 2019), use a simpler method: one only needs to use samples to lower-bound the probability  $p_c$  that the base classifier returns the top class. One can then upper bound all other class probabilities by observing that  $\forall c', p_{c'} \leq 1 - p_c$ . In other words, rather than determining whether  $c$  will stay the plurality class at an adversarial point, one instead determines whether  $c$  will stay the *majority* class. This works well if the probability that  $f$  returns a class other than  $c$  is concentrated in a single ‘‘runner-up’’ class, which (Cohen et al., 2019) finds to be typical, at least in the  $L_2$  smoothing case. This is also the estimation method used by (Levine & Feizi, 2019a) for  $L_0$  certificates: this is why, when describing that method in the Section 2.1, we gave the condition for certification as  $p_c > 0.5 + \Delta$ . In our deterministic method, we can use a

less strict condition, that  $\forall c', p_c - p_{c'} > 2\Delta$ . (As detailed in the above proof, we can sometimes even certify in the *equality* case, if it is assured that, by stable sorting,  $c$  will be selected if there is a tie between the class probabilities at the distorted point.)

In this work, we sidestep the estimation problem entirely by computing the population probabilities exactly. However, by avoiding the assumption of (Cohen et al., 2019), that all probability not assigned to  $c$  is instead assigned to a single adversarial class, we can make an important additional optimization: we can add an ‘abstain’ option. If there is no compelling evidence for any particular class in an ablated image (i.e., if all logits are below a threshold value  $\theta$ ), our classifier abstains, not incrementing the ‘Counts’ for any class. This prevents blocks which contain no information from being assigned to an arbitrary, likely incorrect class. Table 5 shows that this significantly increases the certified accuracy. Our threshold system also allows the base classifier to select *multiple* classes, if there is strong evidence for each of them. This is intended to increase certified accuracy in the case of a large number of classes (i.e., ImageNet), where the top-1 accuracy of the base classifier might be very low: if the correct class consistently occurs within the top several classes, it may still be possible to certify robustness.

### 3. Results

#### 3.1. MNIST, CIFAR-10, ImageNet

Certified robustness against patch attacks is presented for  $5 \times 5$  patches on MNIST and CIFAR-10 in Tables 5 and 4, respectively, and for ImageNet for  $42 \times 42$  patches in Table 3. On MNIST and CIFAR-10, we tested using both block and column smoothing, for all block/column sizes for which certificates are mathematically possible ( $\Delta < .5$ ). (On MNIST, we also tested smoothing with rows rather than columns, with slightly worse results: this is presented in Appendix A.) On ImageNet (Table 3), we tested with column smoothing, as this worked best for both CIFAR-10 and MNIST. We selected to use columns of width 25, on the rough intuition that, averaging over CIFAR-10 and MNIST, the optimal column width for smoothing was at  $s = .6m$ : further exploration of this parameter space would likely yield improved certificates on ImageNet.

#### 3.2. Advantages due to De-randomization

As discussed in Section 2.6, there are two benefits to de-randomization: first, we can eliminate estimation error, and second, it allows the classifier to abstain or select multiple classes without complicating estimation. In order to distinguish these effects, we present in Table 6 the MNIST column certificates using *randomized* column smoothing (with the estimation scheme from (Cohen et al., 2019)), ver-

	Clean Accuracy	Certified Accuracy
$s = 25, \theta = 0.1$	44.0%	12.0%
$s = 25, \theta = 0.2$	<b>43.1%</b>	<b>14.5%</b>
$s = 25, \theta = 0.3$	42.3%	13.8%
$s = 25, \theta = 0.4$	40.9%	12.3%

Table 3. Certified robustness to  $42 \times 42$  patch adversarial attacks using Column smoothing on ImageNet, with column width  $s = 25$ . We test on 1000 images from the ILSVRC2012 validation set.

Block Size $s$	Clean Accuracy	Certified Accuracy
1	14.53%	12.29%
2	30.08%	21.27%
3	41.95%	28.19%
4	28.86%	19.35%
5	58.52%	38.04%
6	68.58%	46.06%
7	71.99%	47.61%
8	74.87%	50.16%
9	79.08%	53.34%
10	82.42%	54.67%
11	84.79%	55.22%
12	<b>86.44%</b>	<b>55.69%</b>
13	88.22%	54.84%
14	89.67%	54.90%
15	52.99%	90.86%
16	91.96%	49.94%
17	92.28%	45.21%
18	93.56%	34.10%
Column Size $s$	Clean Accuracy	Certified Accuracy
1	72.63%	51.11%
2	77.49%	54.05%
3	81.78%	56.72%
4	<b>83.93%</b>	<b>57.83%</b>
5	85.94%	56.01%
6	87.85%	56.22%
7	89.58%	54.63%
8	90.49%	53.03%
9	91.19%	50.6%
10	91.46%	49.64%
11	92.27%	46.67%

Table 4. Certified robustness to  $5 \times 5$  patch adversarial attacks using Block and Column smoothing on CIFAR-10. Values with highest certified accuracies are shown in bold. Note that some models achieve over 90% clean accuracy with over 50% certified robust accuracy. For each configuration, we report accuracies using the  $\theta \in \{0.2, 0.3, 0.4\}$  that yields the highest certified accuracy: results for all  $\theta$ 's are in Appendix C.

## (De)Randomized Smoothing for Certifiable Defense against Patch Attacks

Block Size $s$	$\theta = .2$		$\theta = .3$		$\theta = .4$		Top-1 class (no threshold)	
	Clean Accuracy	Certified Accuracy	Clean Accuracy	Certified Accuracy	Clean Accuracy	Certified Accuracy	Clean Accuracy	Certified Accuracy
1, 2, 3	9.80%	0.00%	9.80%	0.00%	9.80%	0.00%	11.35%	11.35%
4	87.45%	38.15%	86.10%	29.75%	85.95%	19.08%	13.30%	11.35%
5	91.35%	42.66%	90.26%	36.58%	90.43%	26.76%	21.61%	11.58%
6	93.25%	42.67%	92.72%	40.09%	92.61%	33.35%	31.37%	12.23%
7	94.76%	43.86%	94.23%	42.03%	94.29%	35.96%	50.85%	13.69%
8	<b>95.94%</b>	<b>44.00%</b>	95.39%	42.27%	95.44%	36.97%	76.08%	17.81%
9	96.72%	42.04%	96.70%	41.69%	96.61%	37.06%	91.11%	26.58%
10	97.32%	39.98%	97.07%	40.22%	97.09%	36.14%	95.41%	35.27%
11	97.64%	36.67%	97.47%	37.18%	97.46%	32.57%	96.37%	31.65%
12	97.99%	33.42%	97.84%	34.49%	97.93%	30.26%	96.84%	27.20%
13	98.22%	28.66%	98.13%	29.06%	98.25%	22.71%	97.83%	27.79%
14	98.56%	22.24%	98.48%	18.63%	98.48%	14.44%	98.31%	24.16%
15	98.71%	9.13%	98.67%	7.72%	98.7%	5.88%	98.58%	13.02%
Column Size $s$	$\theta = .2$		$\theta = .3$		$\theta = .4$		Top-1 class (no threshold)	
1	93.35%	47.29%	93.13%	47.8%	92.43%	45.64%	50.15%	15.22%
2	96.54%	51.13%	<b>96.66%</b>	<b>52.83%</b>	96.25%	51.81%	72.90%	19.35%
3	97.67%	45.50%	97.49%	46.92%	97.26%	38.52%	81.90%	19.55%
4	97.73%	38.40%	97.67%	32.34%	97.70%	31.72%	84.96%	19.80%
5	98.12%	32.35%	98.11%	25.05%	98.02%	24.66%	93.01%	21.21%
6	98.36%	27.31%	98.26%	20.4%	98.20%	19.81%	95.44%	22.33%
7	98.52%	13.59%	98.53%	15.13%	98.46%	15.27%	97.40%	20.37%
8	98.66%	9.53%	98.60%	10.90%	98.63%	11.15%	97.79%	19.16%
9	98.72%	6.31%	98.72%	7.81%	98.64%	8.16%	98.29%	17.58%

Table 5. Certified robustness to  $5 \times 5$  patch adversarial attacks using Block and Column smoothing on MNIST. Values with highest certified accuracies are shown in bold.

sus deterministic column smoothing without abstentions or multiple-selections: that is to say, counting just the top-1 class returned by the base classifier. The “Top-1” deterministic values are also presented in Table 5, on the right. We see that, while determinism alone provides some benefit, the thresholding system provides an even greater improvement.

Column Size $s$	Deterministic Top-1 Class	Randomized Ablation
1	15.22%	12.41%
2	19.35%	14.55%
3	19.55%	15.46%
4	19.80%	15.32%
5	21.21%	15.56%
6	22.33%	16.48%
7	20.37%	14.79%
8	19.16%	14.97%
9	17.58%	14.12%

Table 6. Comparison of certified accuracy using deterministic versus randomized column smoothing. Figures are for  $5 \times 5$  adversarial patches on MNIST. Note that randomized certificates are probabilistic, with 95% confidence.

	Clean Accuracy	Certified Accuracy
2 columns, $s = 1$	96.39%	39.19%
2 columns, $s = 2$	98.26%	31.08%
3 columns, $s = 1$	97.65%	9.04%
2 blocks, $s = 4$	92.29%	43.45%
3 blocks, $s = 4$	95.04%	41.59%
4 blocks, $s = 4$	96.12%	38.51%

Table 7. Multi-column and multi-block certificates. For each configuration, we report accuracies using the  $\theta \in \{0.2, 0.3, 0.4\}$  that yields the highest certified accuracy: results for all  $\theta$ ’s are in Appendix B. Results are on MNIST, for  $5 \times 5$  patches.

### 3.3. Multiple Blocks, Multiple Bands

In Section 2.2, we argued for using a single contiguous group of pixels on the grounds that, compared to selecting individual pixels, it provides for a smaller risk of intersecting the adversarial patch. However, there may be some benefit to getting information from multiple distinct areas of an image, even if there is some associated increase in  $\Delta$ . Rather than just looking at the extremes of entirely in-



dependent pixels (Table 2) versus a single band or block (Table 5) we also explored, on MNIST, the intermediate case of using a small number of bands or blocks (Table 7). We show all mathematically possible multiple-column certificates on MNIST, as well as several certificates for multiple-blocks with  $s = 4$ . Note that in order to avoid overlapping columns/blocks we select columns/blocks aligned to a grid: details on the certificates (which are deterministic) are provided in Appendix D. Interestingly, while the certificates using multiple columns are far below optimal, the certified accuracy for two blocks is only marginally below the best single-block certified accuracy.

## Conclusion

In this paper, we proposed two related methods for image classification which are provably robust to patch adversarial attacks. These methods, which are adaptations of randomized smoothing, far exceed the current state-of-the-art certified accuracy to patch attacks on CIFAR-10. One of our methods, column smoothing, provides certified robustness on ImageNet comparable to the empirical robustness of state-of-the-art empirical defenses against patch attacks, with very little parameter tuning: it is likely possible to tune this technique to provide even greater certified accuracy.

## References

- Blum, A., Dick, T., Manoj, N., and Zhang, H. Random smoothing might be unable to certify  $\ell_\infty$  robustness for high-dimensional images. *arXiv preprint arXiv:2002.03517*, 2020.
- Brown, T. B., Man, D., Roy, A., Abadi, M., and Gilmer, J. Adversarial patch, 2017.
- Carlini, N. and Wagner, D. Towards evaluating the robustness of neural networks. In *2017 38th IEEE Symposium on Security and Privacy (SP)*, pp. 39–57. IEEE, 2017.
- Chiang, P., Ni, R., Abdelkader, A., Zhu, C., Studor, C., and Goldstein, T. Certified defenses for adversarial patches. In *International Conference on Learning Representations*, 2020. URL <https://openreview.net/forum?id=HyeaSkYYPH>.
- Cohen, J., Rosenfeld, E., and Kolter, Z. Certified adversarial robustness via randomized smoothing. In *International Conference on Machine Learning*, pp. 1310–1320, 2019.
- Eykholt, K., Evtimov, I., Fernandes, E., Li, B., Rahmati, A., Xiao, C., Prakash, A., Kohno, T., and Song, D. Robust physical-world attacks on deep learning visual classification. In *Proceedings of the IEEE Conference on Computer Vision and Pattern Recognition*, pp. 1625–1634, 2018.
- Gowal, S., Dvijotham, K., Stanforth, R., Bunel, R., Qin, C., Uesato, J., Arandjelovic, R., Mann, T., and Kohli, P. On the effectiveness of interval bound propagation for training verifiably robust models. *arXiv preprint arXiv:1810.12715*, 2018.
- Hayes, J. On visible adversarial perturbations & digital watermarking. In *Proceedings of the IEEE Conference on Computer Vision and Pattern Recognition Workshops*, pp. 1597–1604, 2018.
- Karmon, D., Zoran, D., and Goldberg, Y. Lavan: Localized and visible adversarial noise. *arXiv preprint arXiv:1801.02608*, 2018.
- Kumar, A., Levine, A., Goldstein, T., and Feizi, S. Curse of dimensionality on randomized smoothing for certifiable robustness. *arXiv preprint arXiv:2002.03239*, 2020.
- Kurakin, A., Goodfellow, I. J., and Bengio, S. Adversarial examples in the physical world. In *Artificial Intelligence Safety and Security*, pp. 99–112. Chapman and Hall/CRC, 2018.
- Lecuyer, M., Atlidakis, V., Geambasu, R., Hsu, D., and Jana, S. Certified robustness to adversarial examples with differential privacy. In *2019 IEEE Symposium on Security and Privacy (SP)*, pp. 726–742, Los Alamitos, CA, USA, may 2019. IEEE Computer Society. doi: 10.1109/SP.2019.00044. URL <https://doi.ieeecomputersociety.org/10.1109/SP.2019.00044>.
- Lee, G.-H., Yuan, Y., Chang, S., and Jaakkola, T. S. Tight certificates of adversarial robustness for randomly smoothed classifiers. *arXiv preprint arXiv:1906.04948*, 2019.
- Levine, A. and Feizi, S. Robustness certificates for sparse adversarial attacks by randomized ablation. *arXiv preprint arXiv:1911.09272*, 2019a.
- Levine, A. and Feizi, S. Wasserstein smoothing: Certified robustness against wasserstein adversarial attacks. *arXiv preprint arXiv:1910.10783*, 2019b.
- Levine, A., Singla, S., and Feizi, S. Certifiably robust interpretation in deep learning. *arXiv preprint arXiv:1905.12105*, 2019.
- Li, B., Chen, C., Wang, W., and Carin, L. Second-order adversarial attack and certifiable robustness. *arXiv preprint arXiv:1809.03113*, 2018.
- Madry, A., Makelov, A., Schmidt, L., Tsipras, D., and Vladu, A. Towards deep learning models resistant to adversarial attacks. *arXiv preprint arXiv:1706.06083*, 2017.

- Naseer, M., Khan, S., and Porikli, F. M. Local gradients smoothing: Defense against localized adversarial attacks. *2019 IEEE Winter Conference on Applications of Computer Vision (WACV)*, pp. 1300–1307, 2018.
- Rosenfeld, E., Winston, E., Ravikumar, P., and Kolter, J. Z. Certified robustness to label-flipping attacks via randomized smoothing. *arXiv preprint arXiv:2002.03018*, 2020.
- Salman, H., Yang, G., Li, J., Zhang, P., Zhang, H., Razenshteyn, I., and Bubeck, S. Provably robust deep learning via adversarially trained smoothed classifiers. *arXiv preprint arXiv:1906.04584*, 2019.
- Szegedy, C., Zaremba, W., Sutskever, I., Bruna, J., Erhan, D., Goodfellow, I., and Fergus, R. Intriguing properties of neural networks. *arXiv preprint arXiv:1312.6199*, 2013.
- Teng, J., Lee, G.-H., and Yuan, Y.  $\ell_1$  adversarial robustness certificates: a randomized smoothing approach, 2020. URL <https://openreview.net/forum?id=H1lQIgrFDS>.
- Yang, G., Duan, T., Hu, E., Salman, H., Razenshteyn, I., and Li, J. Randomized smoothing of all shapes and sizes. *arXiv preprint arXiv:2002.08118*, 2020.

## A. Results for Row Smoothing

We tested smoothing with rows, rather than columns, on MNIST. This resulted in slightly lower certified accuracy under  $5 \times 5$  patch attacks (45.35% certified accuracy, versus 53.98% using column smoothing). Full results are presented in Table 8.

## B. Results for Multi-column and Multi-block Smoothing for All Tested Values of Parameter $\theta$

In Table 9, we present complete results for multi-column and multi-block smoothing on MNIST, for all tested values of threshold parameter  $\theta$ .

## C. Results on CIFAR-10 for All Tested Values of Parameter $\theta$

In Table 12, we present complete results on CIFAR-10, for all tested values of threshold parameter  $\theta$ .

## D. Certificates for Multi-column and Multi-block Smoothing

For smoothing with multiple blocks or multiple columns, we consider only blocks or columns aligned to a grid starting at the upper-left corner of the image. For example, if using block size  $s = 4$ , we consider only retaining blocks with upper-left corner  $(i, j)$ , where  $i$  and  $j$  are both multiples of 4. This prevents retained blocks from overlapping, and also reduces the (large) number of possible selections of multiple blocks, allowing for derandomized smoothing. Let the number of retained blocks or bands be  $\kappa$ , and, as in the paper, let the block or band size be  $s$ , the image size be  $h \times w$ , and the adversarial patch size be  $m \times m$ .

For the block case, note that there are  $\lceil h/s \rceil \times \lceil w/s \rceil$  such axis-aligned blocks. Of these, the adversarial patch will overlap at most  $(\lceil (m-1)/s \rceil + 1)^2$  blocks. For example, for a  $5 \times 5$  adversarial patch, using block size  $s = 4$ , the adversarial patch will overlap exactly 4 blocks, regardless of position: see Figure 4. When performing derandomized smoothing, we classify all  $\binom{\lceil h/s \rceil \times \lceil w/s \rceil}{\kappa}$  possible choices of  $\kappa$  blocks. Of these classifications, at least

$$\binom{\lceil h/s \rceil \times \lceil w/s \rceil - (\lceil (m-1)/s \rceil + 1)^2}{\kappa}$$

will use none of the at most  $(\lceil (m-1)/s \rceil + 1)^2$  blocks which may be affected by the adversary. Therefore, the number of classifications which might be affected by the adversary is at most:

$$\binom{\lceil h/s \rceil \times \lceil w/s \rceil}{\kappa} - \binom{\lceil h/s \rceil \times \lceil w/s \rceil - (\lceil (m-1)/s \rceil + 1)^2}{\kappa}.$$

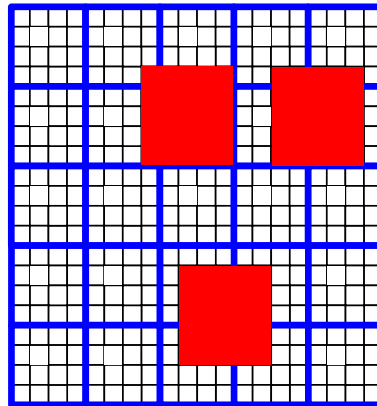


Figure 4. Multi-block smoothing: for a  $5 \times 5$  adversarial patch, using block size  $s = 4$ , the adversarial patch will overlap exactly 4 blocks, regardless of position. Individual pixels are represented by black gridlines. Blocks that may be retained are outlined in blue, and a selection of three possible  $5 \times 5$  adversarial patches are shown in red. Note that this is exact because, in this case,  $m - 1$  is divisible by  $s$ : in other cases, certain choices of adversarial patches may affect fewer than  $(\lceil (m-1)/s \rceil + 1)^2$  blocks.

We can then use the above quantity in place of the variable AffectedBlocks in the certification algorithm (Algorithm 1). This modification, in addition to classifying all  $\binom{\lceil h/s \rceil \times \lceil w/s \rceil}{\kappa}$  selections of  $\kappa$  axis-aligned blocks, is sufficient to adapt the certification algorithm to a multi-block setting.

The column case is similar: there are  $\lceil w/s \rceil$  axis-aligned bands (defined as bands which start at a column index which is a multiple of  $s$ ). Of these, the adversarial patch will overlap at most  $(\lceil (m-1)/s \rceil + 1)$  bands. When performing smoothing, we classify all  $\binom{\lceil w/s \rceil}{\kappa}$  possible choices of  $\kappa$  bands. Of these classifications, at least

$$\binom{\lceil w/s \rceil - (\lceil (m-1)/s \rceil + 1)}{\kappa}$$

will use none of the at most  $(\lceil (m-1)/s \rceil + 1)$  bands which may be affected by the adversary. Therefore, the number of classifications which might be affected by the adversary is at most:

$$\binom{\lceil w/s \rceil}{\kappa} - \binom{\lceil w/s \rceil - (\lceil (m-1)/s \rceil + 1)}{\kappa}.$$

Full results for multi-block and multi-band smoothing are shown in Table 9.

## E. Architecture and Training Details

As discussed in the paper, we used the method introduced by (Levine & Feizi, 2019a) to represent images with pixels ablated: this requires increasing the number of input channels from one to two for greyscale images (MNIST) and

(De)Randomized Smoothing for Certifiable Defense against Patch Attacks

Row Size $s$	$\theta = .2$		$\theta = .3$		$\theta = .4$	
1	88.39%	36.29%	84.75%	33.67%	82.73%	25.46%
2	95.37%	43.25%	<b>93.66%</b>	<b>45.35%</b>	91.89%	42.99%
3	96.13%	41.43%	94.88%	44.76%	93.85%	43.98%
4	96.86%	38.37%	96.09%	42.13%	95.30%	42.05%
5	97.31%	35.38%	96.61%	39.09%	96.05%	39.89%
6	97.26%	31.91%	96.78%	36.53%	96.46%	37.02%
7	97.71%	26.99%	97.28%	32.71%	97.09%	33.43%
8	97.92%	22.76%	97.77%	28.03%	97.64%	29.46%
9	97.93%	17.47%	97.62%	23.90%	97.62%	25.31%

Table 8. Certified robustness to  $5 \times 5$  patch adversarial attacks using Row smoothing on MNIST. Values with highest certified accuracies are shown in bold.

	$\theta = .2$		$\theta = .3$		$\theta = .4$	
	Clean Accuracy	Certified Accuracy	Clean Accuracy	Certified Accuracy	Clean Accuracy	Certified Accuracy
2 columns, $s = 1$	96.57%	38.00%	96.39%	39.19%	96.15%	37.18%
2 columns, $s = 2$	98.26%	31.08%	98.09%	25.01%	98.05%	25.13%
3 columns, $s = 1$	97.67%	7.35%	97.65%	9.04%	97.56%	8.90%
2 blocks, $s = 4$	92.29%	43.45%	91.31%	38.68%	91.16%	29.57%
3 blocks, $s = 4$	95.04%	41.59%	94.45%	39.27%	94.35%	32.66%
4 blocks, $s = 4$	96.12%	38.51%	95.68%	37.50%	95.60%	31.89%

Table 9. Multi-column and multi-block certificates, with results shown for all tested values of parameter  $\theta$ . Results are on MNIST, for  $5 \times 5$  patches.

Training Epochs	400
Batch Size	128
Optimizer	Stochastic Gradient Descent with Momentum
Learning Rate	.01 (Epochs 1-200) .001 (Epochs 201-400)
Momentum	0.9
$L_2$ Weight Penalty	0.0005

Table 10. Training Parameters for MNIST

Training Epochs	350
Batch Size	128
Training Set Preprocessing	Random Cropping (Padding:4) and Random Horizontal Flip
Optimizer	Stochastic Gradient Descent with Momentum
Learning Rate	.1 (Epochs 1-150) .01 (Epochs 151-250) .001 (Epochs 251-350)
Momentum	0.9
$L_2$ Weight Penalty	0.0005

Table 11. Training Parameters for CIFAR-10

from three to six for color images. For MNIST, we used the simple CNN architecture from the released code of (Levine & Feizi, 2019a), consisting of two convolutional layers and three fully-connected layers. For CIFAR-10 and ImageNet, we used modified versions ResNet-18 and ResNet-50, respectively, with the number of input channels increased to six. Training details are presented in Tables 10, 11 and 13.

For randomized smoothing experiments, we follow the empirical estimation methods proposed by (Cohen et al., 2019). We certify to 95% confidence, using 1000 random samples to select the putative top class, and 10000 random samples to lower-bound the probability of this class. For sparse randomized ablation on MNIST, we use released pretrained models from (Levine & Feizi, 2019a).

## F. Proof for Column Smoothing Algorithm (Theorem 2)

For completeness, we include a proof of the correctness of the Column smoothing algorithm (Algorithm 2). This is very similar to the proof of Theorem 1.

*Proof.* Let  $(i', j')$  represent the upper-right corner of the  $m \times m$  patch in which  $\mathbf{x}$  and  $\mathbf{x}'$  differ. Note that the output of  $\text{ABLATE}_{\text{col.}}(\mathbf{x}, s, i)$  will be equal to the output of  $\text{ABLATE}_{\text{col.}}(\mathbf{x}', s, i)$ , unless the band (of width  $s$ ) retained,

(De)Randomized Smoothing for Certifiable Defense against Patch Attacks

Block Size $s$	$\theta = .2$		$\theta = .3$		$\theta = .4$	
	Clean Accuracy	Certified Accuracy	Clean Accuracy	Certified Accuracy	Clean Accuracy	Certified Accuracy
1	14.53%	12.29%	14.28%	12.18%	13.28%	10.45%
2	30.08%	21.27%	25.60%	17.18%	22.61%	13.95%
3	41.95%	28.19%	36.62%	24.48%	32.79%	18.51%
4	28.86%	19.35%	31.22%	19.06%	32.29%	17.33%
5	58.52%	38.04%	57.80%	36.18%	56.03%	29.81%
6	68.58%	46.06%	67.82%	44.51%	66.32%	39.03%
7	71.99%	47.61%	71.87%	47.45%	71.32%	42.96%
8	75.20%	49.79%	74.87%	50.16%	75.61%	47.13%
9	79.30%	52.66%	79.08%	53.34%	79.49%	50.50%
10	82.40%	53.59%	82.42%	54.67%	82.89%	52.31%
11	84.48%	53.43%	84.79%	55.22%	84.95%	53.12%
12	86.39%	53.31%	<b>86.44%</b>	<b>55.69%</b>	86.83%	54.52%
13	88.32%	52.35%	88.22%	54.84%	88.65%	54.08%
14	89.66%	51.77%	89.67%	54.90%	89.94%	53.94%
15	90.63%	50.05%	90.69%	52.99%	90.86%	52.85%
16	91.91%	46.46%	91.94%	49.68%	91.96%	49.94%
17	91.94%	40.85%	92.14%	44.64%	92.28%	45.21%
18	93.42%	29.24%	93.49%	33.10%	93.56%	34.10%
Column Size $s$	$\theta = .2$		$\theta = .3$		$\theta = .4$	
1	72.78%	50.51%	72.63%	51.11%	73.11%	50.19%
2	77.56%	53.33%	77.49%	54.05%	77.75%	53.05%
3	81.75%	55.98%	81.78%	56.72%	81.80%	55.95%
4	83.86%	56.25%	<b>83.93%</b>	<b>57.83%</b>	84.05%	57.08%
5	86.02%	55.25%	85.94%	56.01%	86.03%	55.90%
6	87.80%	54.76%	87.85%	56.22%	88.06%	56.12%
7	89.47%	53.32%	89.58%	54.63%	89.46%	54.50%
8	90.51%	51.56%	90.49%	53.03%	90.45%	53.01%
9	91.30%	48.30%	91.18%	50.41%	91.19%	50.6%
10	91.56%	46.34%	91.49%	49.02%	91.46%	49.64%
11	92.37%	41.86%	92.33%	45.84%	92.27%	46.67%

Table 12. Certified robustness to  $5 \times 5$  patch adversarial attacks using Block and Column smoothing on CIFAR-10, with results shown for all tested values of parameter  $\theta$ . Values with highest certified accuracies are shown in bold.

Training Epochs	60
Batch Size	196
Training Set Preprocessing	Random Horizontal Flip
Optimizer	Stochastic Gradient Descent with Momentum
Learning Rate	.1 (Epochs 1-20) .01 (Epochs 21-40) .001 (Epochs 41-60)
Momentum	0.9
$L_2$ Weight Penalty	0.0005

Table 13. Training Parameters for ImageNet

starting at column  $i$ , intersects with the  $m \times m$  adversarial patch (starting at  $(i', j')$ ). This condition occurs only when both  $i$  is in the range between  $i' - s + 1$  and  $i' + m - 1$ , inclusive. Note that there are  $(s + m - 1)$  values for  $i$  which meet this condition. Therefore  $\text{ABLATE}_{\text{col.}}(\mathbf{x}', s, i) = \text{ABLATE}_{\text{col.}}(\mathbf{x}, s, i)$  in all but  $(s + m - 1)$  cases.

(If  $i' - s + 1 < 0$ , then the intersecting values for  $i$ , taking into account the wrapping behavior of the ABLATE operator, will be  $h - (i' - s + 1)$  through  $h$  and 0 through  $i' + m - 1$ : there are still  $(s + m - 1)$  such values.)

As a consequence,  $f(\text{ABLATE}_{\text{col.}}(\mathbf{x}, s, i))$  will equal  $f(\text{ABLATE}_{\text{col.}}(\mathbf{x}', s, i))$  in all but  $(s + m - 1)$  cases, so the Counts which are incremented will be the same in all but at most  $(s + m - 1)$  (= AffectedBands) iterations. Let  $\text{Counts}_{\mathbf{x}}$  and  $\text{Counts}_{\mathbf{x}'}$  represent the state of the Counts ar-

ray after the main loop of the algorithm on inputs  $\mathbf{x}$  and  $\mathbf{x}'$ , respectively, and similarly define  $c_{\mathbf{x}}$ ,  $c_{\mathbf{x}'}$ , and  $c_{\text{next}_{\mathbf{x}}}$ . Because, for each class  $k$ ,  $\text{Counts}[k]$  is incremented by at most 1 per iteration, we have that:

$$|\text{Counts}_{\mathbf{x}}[k] - \text{Counts}_{\mathbf{x}'}[k]| \leq \text{AffectedBands}. \quad (4)$$

If  $\text{Counts}_{\mathbf{x}}[c_{\mathbf{x}}] > \text{Counts}_{\mathbf{x}}[c_{\text{next}_{\mathbf{x}}}] + 2 \times \text{AffectedBands}$ , then by sorting, we have that for all classes  $k \neq c_{\mathbf{x}}$ ,  $\text{Counts}_{\mathbf{x}}[c_{\mathbf{x}}] > \text{Counts}_{\mathbf{x}}[k] + 2 \times \text{AffectedBands}$ . Then by Equation 4,  $\text{Counts}_{\mathbf{x}'}[c_{\mathbf{x}}] > \text{Counts}_{\mathbf{x}'}[k]$ , and so  $c_{\mathbf{x}'} = c_{\mathbf{x}}$ .

If  $\text{Counts}_{\mathbf{x}}[c_{\mathbf{x}}] = \text{Counts}_{\mathbf{x}}[c_{\text{next}_{\mathbf{x}}}] + 2 \times \text{AffectedBands}$  and  $c_{\mathbf{x}} < c_{\text{next}_{\mathbf{x}}}$  then for all  $k \neq c_{\mathbf{x}}$ ,  $\text{Counts}_{\mathbf{x}}[c_{\mathbf{x}}] \geq \text{Counts}_{\mathbf{x}}[k] + 2 \times \text{AffectedBands}$ . In the inequality case, we already have that  $\text{Counts}_{\mathbf{x}'}[c_{\mathbf{x}}] > \text{Counts}_{\mathbf{x}'}[k]$ . For the equality case, consider any class  $k$  for which  $\text{Counts}_{\mathbf{x}}[c_{\mathbf{x}}] = \text{Counts}_{\mathbf{x}}[k] + 2 \times \text{AffectedBands}$ . Note that  $\text{Counts}_{\mathbf{x}}[c_{\text{next}_{\mathbf{x}}}] = \text{Counts}_{\mathbf{x}}[k]$  and also, by stable sorting of  $\text{Counts}_{\mathbf{x}}$ ,  $c_{\text{next}_{\mathbf{x}}} \leq k$ . Then because  $c_{\mathbf{x}} < c_{\text{next}_{\mathbf{x}}}$ , we have that  $c_{\mathbf{x}} < k$ . By Equation 4,  $\text{Counts}_{\mathbf{x}'}[c_{\mathbf{x}}] \geq \text{Counts}_{\mathbf{x}'}[k]$ . Then, by stable sorting of  $\text{Counts}_{\mathbf{x}'}$ ,  $c_{\mathbf{x}'} = c_{\mathbf{x}}$   $\square$